



# Tau filaments from amyotrophic lateral sclerosis/parkinsonism-dementia complex adopt the CTE fold

Chao Qi<sup>a,1</sup> , Bert M. Verheijen<sup>b,1</sup>, Yasumasa Kokubo<sup>c,1</sup> , Yang Shi<sup>a,1,2</sup>, Stephan Tetter<sup>a</sup>, Alexey G. Murzin<sup>a</sup>, Asa Nakahara<sup>d</sup> , Satoru Morimoto<sup>e</sup>, Marc Vermulst<sup>b</sup>, Ryogen Sasaki<sup>f</sup> , Eleonora Aronica<sup>g</sup>, Yoshifumi Hirokawa<sup>e</sup> , Kiyomitsu Oyanagi<sup>h</sup> , Akiyoshi Kakita<sup>d</sup> , Benjamin Ryskeldi-Falcon<sup>a</sup>, Mari Yoshida<sup>i</sup>, Masato Hasegawa<sup>j</sup>, Sjors H. W. Scheres<sup>a,3</sup> , and Michel Goedert<sup>a,3</sup>

Edited by John F. Crary, Icahn School of Medicine at Mount Sinai, New York, NY; received April 26, 2023; accepted October 31, 2023 by Editorial Board Member Peter L. Strick

**The amyotrophic lateral sclerosis/parkinsonism-dementia complex (ALS/PDC) of the island of Guam and the Kii peninsula of Japan is a fatal neurodegenerative disease of unknown cause that is characterized by the presence of abundant filamentous tau inclusions in brains and spinal cords. Here, we used electron cryo-microscopy to determine the structures of tau filaments from the cerebral cortex of three cases of ALS/PDC from Guam and eight cases from Kii, as well as from the spinal cord of two of the Guam cases. Tau filaments had the chronic traumatic encephalopathy (CTE) fold, with variable amounts of Type I and Type II filaments. Paired helical tau filaments were also found in three Kii cases and tau filaments with the corticobasal degeneration fold in one Kii case. We identified a new Type III CTE tau filament, where protofilaments pack against each other in an antiparallel fashion. ALS/PDC is the third known tauopathy with CTE-type filaments and abundant tau inclusions in cortical layers II/III, the others being CTE and subacute sclerosing panencephalitis. Because these tauopathies are believed to have environmental causes, our findings support the hypothesis that ALS/PDC is caused by exogenous factors.**

neurodegenerative disease | amyotrophic lateral sclerosis-parkinsonism dementia complex (ALS/PDC) | tau filament assembly | chronic traumatic encephalopathy tau fold

Amyotrophic lateral sclerosis/parkinsonism-dementia complex (ALS/PDC or lytico-bodig) is a fatal disease found in the Chamorro population of Guam (1–4), some families on the Kii peninsula of Japan (5, 6), and the Auyu and Jakai people of New Guinea (7). Abundant tau inclusions are present in nerve cells in brains and spinal cords (6, 8, 9) and are enriched in cortical layers II/III (10, 11). Tau inclusions are also found in some glial cells (12). They consist of amyloid filaments that are made of all six brain tau isoforms in a hyperphosphorylated state (8, 13). More variably, assembled A $\beta$ ,  $\alpha$ -synuclein, and TDP-43 accumulate too (11, 14, 15).

The cause of ALS/PDC is unknown, but it is not a simple genetic disorder in an island-bound geographic isolate (16–18). Exogenous factors may play a role in disease aetiology and pathogenesis, supported by the finding that migrants from the Philippines can develop ALS/PDC after living on Guam for more than two decades (19). With increased Westernisation, the incidence of ALS/PDC is decreasing (20). High prevalence of a retinopathy, called linear retinal pigment epitheliopathy (LRPE), has been reported in Guam and Kii ALS/PDC (21, 22), similar to infestation by a migrating parasite larva. Both disorders have declined in parallel, suggesting a possible link between ALS/PDC and LRPE.

Tau filaments made of all six brain isoforms in a hyperphosphorylated state are also found in Alzheimer's disease (AD) and in chronic traumatic encephalopathy (CTE) (23, 24). They are found predominantly in cortical layers V/VI in AD (25) and in layers II/III in CTE (26). The latter is caused by repetitive head impacts or exposure to blast waves (27). By cryo-EM, we have shown that tau filaments from AD and CTE each consist of two identical C-shaped protofilaments that comprise residues 306 to 378 (in the numbering of the 441 amino acid tau isoform) (28–30). They differ by the presence of a hydrophobic cavity in the CTE fold, which encloses a nonproteinaceous density of unknown identity that may be involved in giving rise to this fold. Besides AD, the Alzheimer tau fold also characterizes primary age-related tauopathy, familial British dementia, familial Danish dementia, and some prion protein amyloidoses (31, 32). The CTE tau fold is also characteristic of subacute sclerosing panencephalitis (SSPE), which is a fatal disorder of the central nervous system that is a rare consequence of infection with measles virus and begins after a symptom-free period of several years (33, 34). Tau inclusions in SSPE are also enriched in cortical layers II/III (35). Here, we report that the CTE

## Significance

A neurodegenerative disease of unknown cause on the island of Guam and the Kii peninsula of Japan has been widely studied, because patients can suffer from the combined symptoms of motor neuron disease, parkinsonism, and dementia. Abnormal filamentous inclusions made of tau protein characterize this amyotrophic lateral sclerosis/parkinsonism-dementia complex (ALS/PDC) and their formation closely correlates with neurodegeneration. Here, we have used electron cryo-microscopy to show that tau filaments from ALS/PDC are identical to those from chronic traumatic encephalopathy (CTE), a disease caused by repetitive head impacts or blast waves. CTE tau filaments are also found in subacute sclerosing panencephalitis, which is a rare consequence of measles infection. ALS/PDC may therefore also be caused by environmental factors.

The authors declare no competing interest.

This article is a PNAS Direct Submission. J.F.C. is a guest editor invited by the Editorial Board.

Copyright © 2023 the Author(s). Published by PNAS. This open access article is distributed under [Creative Commons Attribution License 4.0 \(CC BY\)](https://creativecommons.org/licenses/by/4.0/).

<sup>1</sup>C.Q., B.M.V., Y.K., and Y.S. contributed equally to this work.

<sup>2</sup>Present address: Liangzhu Laboratory, Ministry of Education Frontier Science Center for Brain Science and Brain-machine Integration, State Key Laboratory of Brain-machine Intelligence, Zhejiang University, Hangzhou, 311121, China.

<sup>3</sup>To whom correspondence may be addressed. Email: [scheres@mrc-lmb.cam.ac.uk](mailto:scheres@mrc-lmb.cam.ac.uk) or [mg@mrc-lmb.cam.ac.uk](mailto:mg@mrc-lmb.cam.ac.uk).

This article contains supporting information online at <https://www.pnas.org/lookup/suppl/doi:10.1073/pnas.2306767120/-/DCSupplemental>.

Published December 15, 2023.

fold is typical of tau filaments extracted from brains and spinal cords of individuals with Guam and Kii ALS/PDC, suggesting that similar molecular mechanisms underlie these diseases.

## Results

### Structural Characterization of Filaments from Guam ALS/PDC.

We used cryo-EM to characterize filaments from the frontal cortex of three cases of Guam ALS/PDC and the spinal cord of cases 2 and 3 (Fig. 1 and *SI Appendix*, Figs. S1–S5 and Table S1). We used optimized extraction procedures (36) to deal with the limiting amounts of brain and spinal cord samples that were available for this study (0.03 to 0.4 g per case). Staining with antitau antibody AT8 showed abundant neurofibrillary tangles (intracellular and extracellular) in frontal cortex (*SI Appendix*, Fig. S6). As described (12), tau inclusions were also found in astrocytes and oligodendrocytes, with astrocytic inclusions mostly in subpial and perivascular areas.

Tau filaments with the CTE fold were present in all cases. The frontal cortex from case 1 contained a mixture of Type I and Type II filaments, whereas that from cases 2 and 3 had only Type I filaments. The spinal cord from case 2 had only Type II filaments, whereas that from case 3 contained a mixture of Type I and Type II filaments. In addition to tau filaments, we also observed singlets and doublets of transmembrane protein 106B (TMEM106B) filaments (fold I) in the frontal cortex from cases 1 and 2, and TMEM106B singlets (fold I) in the spinal cord from case 2 (Fig. 1 and *SI Appendix*, Figs. S1 and S2). The frontal cortex from case 2 also contained Type II A $\beta$ 42 filaments (Fig. 1 and *SI Appendix*,

Figs. S1 and S2), like those that were described in brain extracts from cases of AD and other diseases (36). For several filament types, there were insufficient images for de novo three-dimensional reconstruction to high resolution. Their identification was based on 2D class averages (Fig. 1 and *SI Appendix*, Fig. S1).

High-resolution structure determination confirmed that the tau filament structures from Guam ALS/PDC are identical to those from CTE (Fig. 2*A*). The rmsd of C $\alpha$  atoms in one rung of the filaments between Type I filaments from the spinal cord of Guam case 3 and those from CTE (PDB:6NWP) was 0.28 Å; the rmsd between Type II filaments from the frontal cortex of Guam case 1 and those from CTE (PDB:6NWQ) was 1.36 Å.

In the spinal cord of Guam case 3, we found a small proportion of filaments (less than 10%) with a previously unobserved structure, which we named CTE Type III tau filaments (Figs. 1 and 2*B* and *SI Appendix*, Figs. S2 and S5). Like CTE Type I and Type II filaments, Type III filaments consist of two protofilaments with the CTE fold, spanning residues K274–R379 of three-repeat tau and S305–R379 of four-repeat tau, and harboring an additional density in the  $\beta$ -helix region. The mirror-like arrangement of protofilaments in the cross-section indicates that they adopt opposite polarities in the filaments, unlike Type I and Type II filaments. The protofilament interface consists of residues <sup>323</sup>GSLGNIH<sup>329</sup> from both protofilaments, like in the CTE Type I filament interface. However, they form a different, staggered parallel zipper, in which the side chains of S324 and N327 of both protofilaments intercalate and form hydrogen bonds with the main chain groups of opposite protofilaments (Fig. 2*B*). CTE Type III tau filaments were also found in a new, bigger cryo-EM dataset of filaments

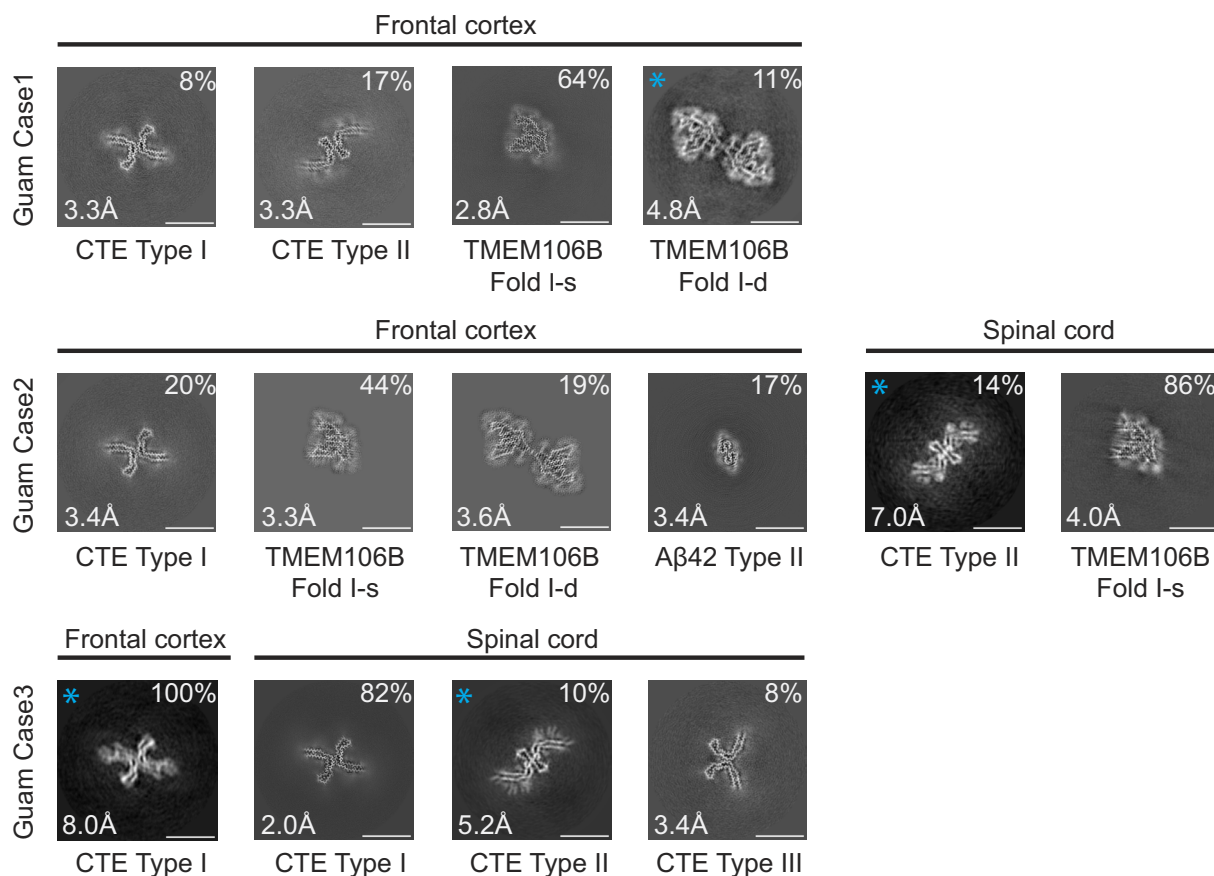


**Fig. 1.** Cross-sections perpendicular to the helical axis of cryo-EM structures of filaments from the frontal cortex and spinal cord of three cases of Guam ALS/PDC, with a projected thickness of approximately one rung along the helical axis. For the filament types indicated with an asterisk, there were insufficient images for high-resolution reconstruction; identification of filament types was also based on 2D class averages. Filament types are indicated, as are structural resolutions and percentages for each type. (Scale bar, 10 nm.)

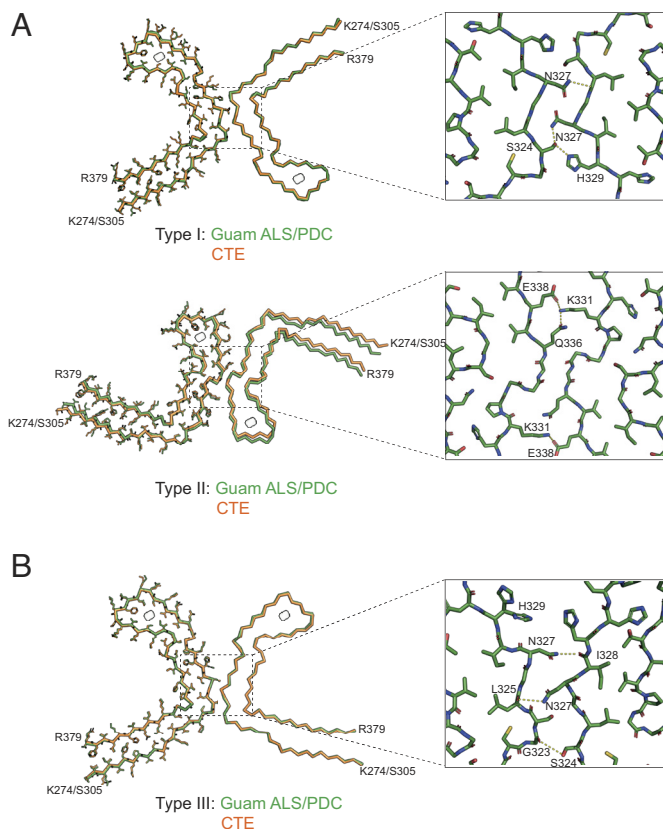


**Fig. 2.** Comparison of tau filaments from Guam ALS/PDC and CTE. (A) Overlays of CTE Type I filaments (Top) and CTE Type II filaments (Bottom) from Guam ALS/PDC (green) and CTE (orange), with one protofilament shown in all atoms and the other protofilament shown as backbone. Insets: Zoomed-in views of the protofilament interfaces of both types of filaments. (B) Overlay of CTE Type III filaments from Guam ALS/PDC (green) and CTE (orange), shown as in (A). Inset: Zoomed-in view of the protofilament interface of CTE Type III filaments.

from the temporal cortex of an individual with CTE (case 2 in ref. 30) (*SI Appendix, Fig. S5*), indicating that they are not restricted to Guam ALS/PDC. Their 2.7 Å resolution structure revealed two alternative conformations of the side chain of H329 in one of the two protofilaments; in one conformation, its imidazole group comes into contact with the imidazole group of H329 from the opposite protofilament (Fig. 2B and *SI Appendix, Fig. S5B*). The low abundance of CTE Type III tau filaments may explain why they were not observed in the smaller cryo-EM datasets of other samples from ALS/PDC.

**Structural Characterisation of Filaments from Kii ALS/PDC.** We analyzed extracts from temporal cortex of eight cases of ALS/PDC from the Kii peninsula (Fig. 3 and *SI Appendix, Figs. S1–S4* and Table S1). We used the standard tau filament extraction method (37) for all eight cases, and the optimised procedure (36) also for cases 6 to 8. Staining with AT8 showed the presence of abundant neurofibrillary tangles that were particularly abundant in cortical layers II/III (*SI Appendix, Fig. S7*). Tau-positive astrocytes and coiled bodies were also present. Case 8 has previously been shown to exhibit astrocytic plaque-like structures and threads, reminiscent of corticobasal degeneration (11).

Using the standard extraction method, all eight samples from the Kii peninsula contained tau filaments with the CTE fold. Case 8 had only Type II filaments; all other cases had a mixture of Type I and Type II filaments. Cases 4 and 5 also contained tau-paired helical filaments (PHFs), like those from AD and other conditions

(28, 29, 31, 32). We did not observe A $\beta$  filaments in any of the Kii cases. High-resolution structure determination showed that the structures of tau filaments from Kii ALS/PDC are also identical to those from CTE (Fig. 3B). The rmsd between Type I filaments from Kii case 2 and those from CTE (PDB:6NWP) was 0.38 Å; the rmsd between Type II filaments from Kii case 2 and those from CTE (PDB:6NWQ) was 1.37 Å.

Using the optimized extraction procedures that were also used for the Guam cases (36), in addition to the filament types described above, we observed tau PHFs for case 7 and TMEM106B Fold III-s filaments for case 8. In agreement with ref. 11, we also observed filaments reminiscent of  $\alpha$ -synuclein filaments from Lewy bodies (38) for case 6 (*SI Appendix, Fig. S1*). These filaments did not show an observable twist, and we were not able to determine their three-dimensional structure. We also observed Corticobasal degeneration (CBD) Type I and CBD Type II tau filaments for case 8 (Fig. 3), consistent with the presence of astrocytic plaque-like structures (11, 39, 40).

## Discussion

Abundant filamentous amyloid inclusions that are made of all six brain tau isoforms are characteristic of ALS/PDC (8, 13). Immunoblotting of sarkosyl-insoluble tau from some of the Kii cases used here has been described previously (6, 13). We now show that tau filaments from Guam and Kii ALS/PDC adopt the CTE fold (30) in brain and spinal cord. We recently showed that tau filaments from SSPE also adopt the CTE fold (33).

The observation that specific tau filament folds characterise different diseases suggests that filament structure may provide a handle to study disease (41). For example, different cellular environments may lead to the formation of distinct structures. The observation that filaments of ALS/PDC are identical to those from CTE and SSPE thus suggests that filaments may form under similar circumstances in these diseases. It follows that the molecular mechanisms that cause tau assembly in ALS/PDC may be similar to those at work in CTE and SSPE. The latter two are probably caused by environmental factors, in the form of repetitive head injuries and measles infection, respectively. Neuroinflammation may be important in both diseases. Exogenous factors may also be causal in Guam and Kii ALS/PDC, with a possible role for parasitic infestation (21, 22).

As in CTE (26) and SSPE (35), more filamentous tau inclusions in ALS/PDC of Guam and Kii are found in layers II/III of the cerebral cortex than in layers V/VI (10, 11). This is unlike AD, where tau inclusions are more abundant in layers V/VI (25). The presence of Alzheimer and CTE tau folds correlates with these differences. It suggests that the CTE fold may also form in other diseases with a predominance of tau inclusions in cortical layers II/III that are believed to be caused by environmental factors, such as postencephalitic parkinsonism (42) and nodding syndrome (43).

The CTE tau fold differs from the Alzheimer fold by having a more open conformation of the  $\beta$ -helix region, which contains an internal density of unknown identity (30). In the presence of NaCl, recombinant tau comprising residues 297 to 391 assembled into filaments with the CTE fold, but in its absence, the Alzheimer tau fold formed (44). It remains to be seen how this difference relates to human brains.

Besides tau filaments with the CTE fold, we also observed tau PHFs in three cases from the Kii peninsula and tau filaments with the CBD fold in one case. Type II A  $\beta$ 42 filaments were present in one case from Guam. Senile plaques have been described in around 60% of cases of Guam ALS/PDC (15) and assembly of A $\beta$  is believed to be part of the disease process (45). Alternatively, these changes may be age-related. This was probably also the reason for the presence of TMEM106B



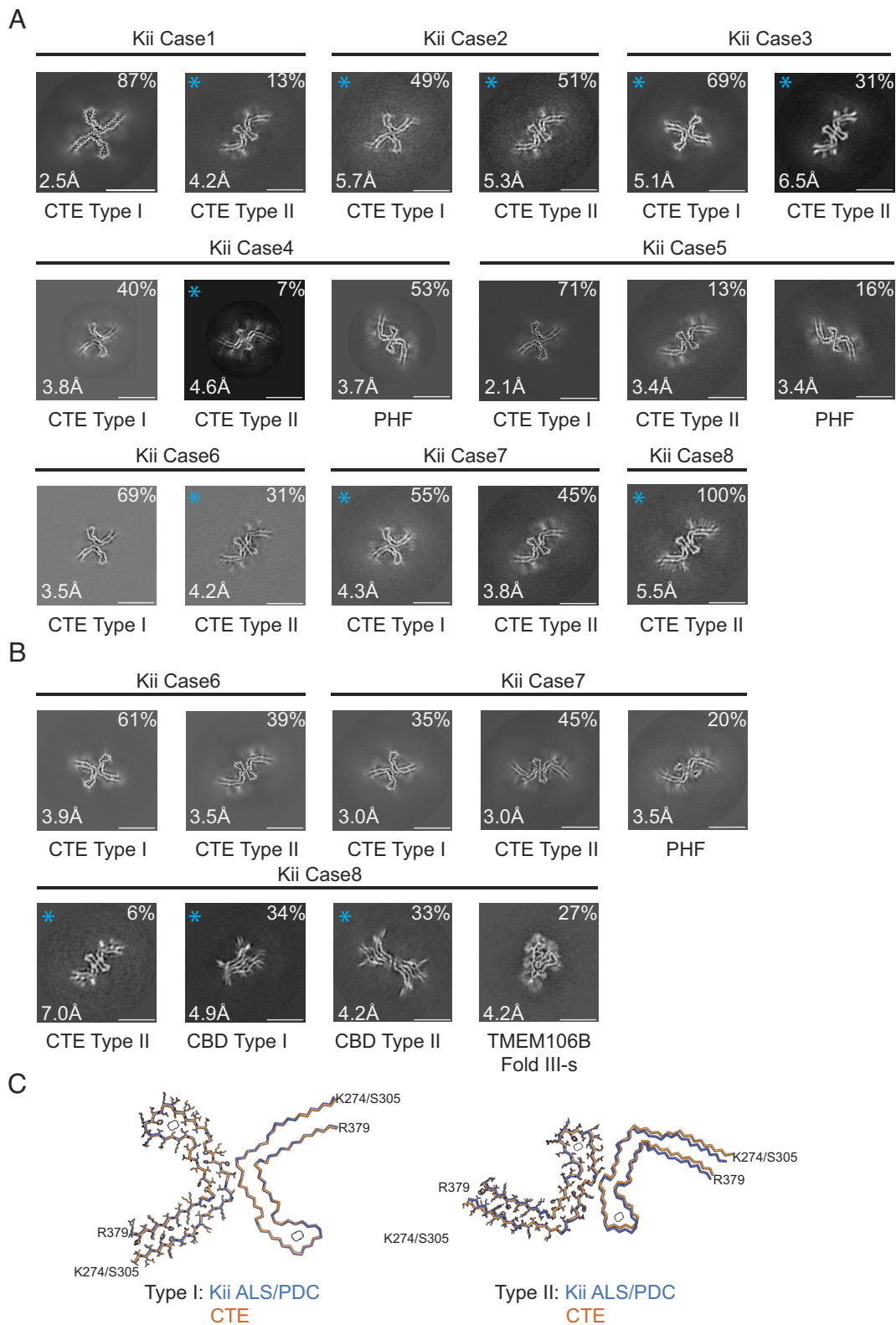


**Fig. 3.** Cross-sections of cryo-EM structures of filaments from Kii ALS/PDC and comparison of tau filaments with those from CTE. (A) Cross-sections perpendicular to the helical axis of cryo-EM structures of filaments from eight cases of Kii ALS/PDC, with a projected thickness of approximately one rung along the helical axis. (B) Cross-sections of filaments from Kii ALS/PDC cases 6, 7, and 8, using the optimised extraction protocol. For the filament types indicated with an asterisk, there were insufficient images for high-resolution reconstruction; identification of filament types was also based on 2D class averages. Filament types are indicated, as are structural resolutions and percentages for each type. (Scale bar, 10 nm.) (C) Overlay of CTE Type I filaments (Left) and Type II filaments (Right) from Kii ALS/PDC (blue) and CTE (orange), shown as in Fig. 2.

filaments (46, 47) in two cases from Guam and one case from the Kii peninsula. It is possible that A $\beta$  and TMEM106B filaments were lost during the extraction method used for some of the Kii

in addition to tau, also A $\beta$ ,  $\alpha$ -synuclein and TDP-43 inclusions have been implicated in the pathogenesis of ALS/PDC (11, 14, 15). We found filaments that were reminiscent of  $\alpha$ -synuclein filaments in one

of the Kii cases. We did not observe TDP-43 filaments in any of the cases from Guam or the Kii peninsula. However, our results with two different extraction protocols for three of the Kii cases illustrate that it would be imprudent to conclude that certain filament types are not present in a brain if they are not observed with a given extraction method.

The greater heterogeneity of amyloid filaments, when compared to CTE and SSPE, probably reflects the fact that ALS/PDC is a multiple proteinopathy based on neuropathology, as suggested for cases from the Kii peninsula (11).

In conclusion, we demonstrate the presence of tau filaments with the CTE fold in cases of ALS/PDC from the island of Guam and the Kii peninsula. Type I and/or Type II CTE filaments were present in brains and spinal cords. We also describe the new CTE Type III tau filament, in which two protofilaments pack with opposite polarities. The presence of tau filaments with the CTE fold supports the hypothesis that ALS/PDC is caused by exogenous factors.

## Materials and Methods

**Cases of ALS/PDC.** Three cases of ALS/PDC from the island of Guam and eight cases from the Kii peninsula were investigated (*SI Appendix, Table S1*). The Guam cases have not been reported before; we used tissues from two Chamorro males and one 1/2 Chamorro, 1/2 Filipina female with long-standing dementia and Parkinson's disease, in the absence of a family history of disease. They belonged to the PDC subtype, where some tau inclusions can be found in the spinal cord (48). They died aged 68 (case 1) and aged 73 (cases 2 and 3). The cases from the Kii peninsula have been published (11). Three individuals (cases 1, 2, and 5) belonged to the ALS subtype and five (cases 3, 4, and 6–8) to the PDC subtype. The ages at death were ALS subtype, 63, 76, and 77 y; PDC subtype, 60, 70, 71, 74, and 74 y. The duration of illness varied between 1 and 14 y. There was no history of head injury or measles infection in either the Guam or the Kii cases of ALS/PDC. This study was approved by the Ethics Committees of the Universities of Shinshu (3233 and 5108), Niigata (2020–0019), and Mie (2592).

**Immunohistochemistry.** Brains were fixed in 20% buffered formalin, cut into coronal sections, and paraffin-embedded. Sections (4.5  $\mu\text{m}$ ) were incubated overnight at room temperature with antibody AT8, which is specific for pS202 and pT205 tau (1:5,000, Innogenetics) (49). To reveal the signal, the Envision plus kit (Dako) was used, with diaminobenzidine tetrahydrochloride (Sigma-Aldrich) as chromogen. Some sections from Kii cases of ALS/PDC were also stained with Gallyas-Braak silver (50).

**Filament Extraction.** For the Guam ALS/PDC cases, we used an optimized extraction procedure, which allowed us to handle small amounts of brain samples (36). Sarkosyl-insoluble material was extracted from the frontal cortex (cases 1 to 3) and spinal cord (cases 2 and 3). The tissues (less than 400 mg) were homogenized in 3 mL buffer A (10 mM Tris-HCl, pH 7.5, 0.8 M NaCl, 10% sucrose, and 1 mM EGTA), brought to 2% sarkosyl, and incubated for 30 min at 37 °C. The samples were centrifuged at 7,000 g for 10 min, followed by spinning the supernatants at 100,000 g for 60 min. The pellets were resuspended in 100  $\mu\text{L}$ /g of buffer B (20 mM Tris-HCl, pH 7.4, 100 mM NaCl) for cryo-EM analysis.

For all eight ALS/PDC cases from the Kii peninsula, filaments were extracted using the standard tau extraction method (37), with minor modifications. After incubation in 2% sarkosyl, the samples were sonicated (TAITEC ultrasonic homogeniser VP-55, level 7) for 15 s and, following a 10 min centrifugation at 27,000 g, supernatants were centrifuged at 257,400 g for 30 min at 25 °C. The pellets were then resuspended in 900  $\mu\text{L}$ /g buffer A with 1% sarkosyl and centrifuged at 166,000 g for 20 min at 25 °C. For cases 6, 7, and 8 from the Kii peninsula, filaments were also extracted using the optimized procedure used for the Guam cases (36). Filaments from the CTE brain (case 2 in ref. 30) were extracted using a procedure that was developed for the extraction of TDP-43 filaments, as described (51).

**Electron Cryo-Microscopy.** Three microliters of the sarkosyl-insoluble fractions were applied to glow-discharged (Edwards S150B) holey carbon grids

(Quantifoil Au R1.2/1.3, 300 mesh) that were plunge-frozen in liquid ethane using a VitroBot Mark IV (Thermo Fisher Scientific) at 100% humidity and 4 °C. Cryo-EM images were collected on a Titan Krios electron microscope operated at 300 kV and equipped with a Falcon-4 or a K3 direct electron detector. Images were recorded in electron event representation (EER) format (52) for Falcon-4 (6 s) and Tif format for K3 (1 s), with a total dose of 40  $\text{e}/\text{\AA}^2$  and a pixel size of 0.824  $\text{\AA}$  (Falcon-4) or 0.826  $\text{\AA}$  (K3).

**Helical Reconstruction.** Datasets were processed in RELION using standard helical reconstruction (53). Movie frames were gain-corrected, aligned, and dose-weighted using RELION's own motion correction program (54). Contrast transfer function (CTF) parameters were estimated using CTFFIND4-1 (55). Filaments were picked manually. For the analysis of filament types and the generation of initial three-dimensional models, segments were extracted with a box size of 1,024 pixels and down-scaled to 256 pixels. Reference-free 2D classification was performed to discard suboptimal images and measure cross-over distances for initial model calculation using `relion_helix_inimodel2d` (56). For high-resolution refinement, selected segments were extracted with a box size of 400 pixels, with the original pixel size. 3D auto-refinements were performed with optimization of the helical twist and rise parameters once resolutions extended beyond 4.7  $\text{\AA}$ . To improve the resolution, Bayesian polishing and CTF refinement were performed (57). Final maps were sharpened using standard postprocessing procedures in RELION and resolution estimates were calculated based on the Fourier shell correlation (FSC) between two independently refined half-maps at 0.143 (58).

**Model Building and Refinement.** For maps with resolutions beyond 4  $\text{\AA}$ , atomic models were built manually in Coot (59), based on published structures [CTE type I, PDB:6NWP; CTE type II, PDB:6NWQ; TMEM106B fold I-s, PDB:7QVC; TMEM106B fold I-d, PDB:7QVF; Type II A $\beta$ 42, PDB:7Q4M (30, 36, 41)]. Model refinements were performed using *Servalcat* (60) and REFMAC5 (61, 62). Models were validated with MolProbity (63). Figures were prepared with ChimeraX (64) and Pymol (Schrodinger, LLC.). See *SI Appendix, Tables S2 and S3* for further details.

**Data, Materials, and Software Availability.** Cryo-EM maps have been deposited in the Electron Microscopy Data Bank (EMDB) with the following accession numbers: EMD-17171 (65), EMD-17173 (66), EMD-17174 (67), EMD-17175 (68), EMD-17176 (69), EMD-17177 (70), EMD-17178 (71), EMD-17179 (72), EMD-17180 (73), and EMD-17181 (74). Corresponding refined atomic models have been deposited in the Protein Data Bank (PDB) under the following accession numbers: 8OT6 (75), 8OTC (76), 8OT9 (77), 8OTD (78), 8OTE (79), 8OTF (80), 8OTG (81), 8OTH (82), 8OTI (83), and 8OTJ (84). Please address requests for materials to the corresponding authors.

**ACKNOWLEDGMENTS.** We are grateful to the patients' families for donating brain tissues. We thank members of the Electron Microscopy (EM) facility at the Medical Research Council (MRC) Laboratory of Molecular Biology for support with data acquisition and Jake Grimmett, Toby Darling and Ivan Clayson for help with high-performance computing. We acknowledge Diamond for access and support of the cryo-EM facilities at the U.K. National electron Bio-Imaging Centre, proposal BI31336, funded by the Wellcome Trust, the MRC, and the Biotechnology and Biological Sciences Research Council (BBSRC). This work was funded by the MRC, as part of U.K. Research and Innovation (MC\_UP\_120/25 to B.R.-F., MC\_UP\_A025\_1013 to S.H.W.S. and MC\_U105184291 to M.G.). It was also supported by the U.S. National Institute on Aging (R01AG054641, to M.V. and B.M.V.), a Pilot Award from the Southern California Environmental Health Sciences Center (to M.V. and B.M.V.), the ALS Stichting (to E.A.), the Mie Medical Fund (to Y.K. and S.M.), the Research Committee of CNS Degenerative Diseases (to Y.K.), the Research Committee on Muro Disease (21210301 to Y.K.), the Japan Society for the Promotion of Science (JSPS KAKENHI, JP18K07514 to Y.K. and JP22H04923 to S.M.), the Japan Agency for Medical Research and Development (to Y.K., M.Y., and M.H.), a Swiss National Science Postdoctoral Fellowship (P500PB 206890 to S.T.), and a Collaborative Research Project from the Niigata Brain Research Institute (to A.K.). We acknowledge the contributions of Professor Shigeki Kuzuhara (1944 to 2021) to the study of Kii ALS/PDC. For the purpose of open access, the MRC Laboratory of Molecular Biology has applied a CC-BY public copyright license to any Author Accepted Manuscript version arising.

Author affiliations: \*Medical Research Council, Laboratory of Molecular Biology, Cambridge CB2 0QH, United Kingdom; †Leonard Davis School of Gerontology, University of Southern California, Los Angeles, CA 90089; ‡Graduate School of Regional Innovation Studies, Mie University, Tsu 514-8507, Japan; †Department of Pathology, Brain Research Institute, Niigata University, Niigata 951-8585, Japan; †Department of Oncologic Pathology, Graduate School of Medicine, Mie University, Tsu 514-8507, Japan; †Department of Nursing, Suzuka University of Medical Science, Suzuka 513-8670, Japan; †Department of Neuropathology, Amsterdam University Medical Centers (UMC), University of Amsterdam, Amsterdam Neuroscience, Amsterdam 1105 AZ, The Netherlands; †Department of Brain Disease

Research, Shinshu University School of Medicine, Matsumoto 390-8621, Japan; †Department of Neuropathology, Institute for Medical Science of Aging, Aichi Medical University, Nagakute 480-1195, Japan; and †Department of Brain and Neuroscience, Tokyo Metropolitan Institute of Medical Science, Tokyo 156-8506, Japan

Author contributions: C.Q., Y.S., S.T., and M.H. extracted filaments; B.M.V., Y.K., A.N., S.M., M.V., R.S., E.A., Y.H., K.O., A.K., and M.Y. identified the patients and performed neuropathology; C.Q., Y.S., and S.T. acquired cryo-EM data; C.Q., Y.S., S.T., A.G.M., B.R.-F., and S.H.W.S. did structure determination; S.H.W.S. and M.G. supervised the project; and C.Q., B.M.V., Y.K., Y.S., S.T., A.G.M., B.R.-F., S.H.W.S., and M.G. wrote the paper.

1. H. M. Zimmerman, Memorandum to U.S.N. (Medical Research Unit No. 2, 1945).
2. A. Arnold, D. C. Edgren, V. S. Palladino, Amyotrophic lateral sclerosis: 50 cases observed on Guam. *J. Nerv. Ment. Dis.* **117**, 135–139 (1953).
3. A. Hirano, L. T. Kurland, R. S. Krooth, S. Lessell, Parkinsonism-dementia complex, an endemic disease on the island of Guam. I. Clinical features. *Brain* **84**, 642–661 (1961).
4. A. Hirano, N. Malamud, L. T. Kurland, Parkinsonism-dementia complex, an endemic disease on the island of Guam. II. Pathological features. *Brain* **84**, 662–679 (1961).
5. Y. Yase, N. Matsumoto, K. Azuma, Y. Nakai, H. Shiraki, Amyotrophic lateral sclerosis. Association with schizophrenic symptoms and showing Alzheimer's tangles. *Arch. Neurol.* **27**, 118–128 (1972).
6. S. Kuzuhara *et al.*, Familial amyotrophic lateral sclerosis and parkinsonism-dementia of the Kii peninsula of Japan: Clinical and neuropathological study and Tau analysis. *Ann. Neurol.* **49**, 501–511 (2001).
7. D. C. Gajdusek, A. M. Salazar, Amyotrophic lateral sclerosis and parkinsonian syndromes in high incidence among the Auyu and Jakai people of West New Guinea. *Neurology* **32**, 107–126 (1982).
8. V. Buée-Scherrer *et al.*, Neurofibrillary degeneration in amyotrophic lateral sclerosis/Parkinsonism-dementia complex of guam. immunohistochemical characterization of tau proteins. *Am. J. Pathol.* **68**, 924–932 (1995).
9. M. L. Schmidt *et al.*, Spinal cord neurofibrillary pathology in Alzheimer disease and Guam Parkinsonism-Dementia complex. *J. Neuropathol. Exp. Neurol.* **60**, 1075–1086 (2001).
10. P. R. Hof *et al.*, Amyotrophic lateral sclerosis/parkinsonism-dementia complex of Guam: Quantitative neuropathology, immunohistochemical analysis of neuronal vulnerability, and comparison with related neurodegenerative disorders. *Acta Neuropathol.* **88**, 397–404 (1994).
11. M. Mimuro, M. Yoshida, S. Kuzuhara, Y. Kokubo, Amyotrophic lateral sclerosis and parkinsonism-dementia complex of the Hohara focus of the Kii peninsula: A multiple proteinopathy? *Neuropathology* **38**, 98–107 (2018).
12. K. Oyanagi *et al.*, Distinct pathological features of the Gallyas- and Tau-positive glia in the parkinsonism-dementia complex and amyotrophic lateral sclerosis. *J. Neuropathol. Exp. Neurol.* **56**, 308–316 (1997).
13. N. Itoh *et al.*, Biochemical and ultrastructural study of neurofibrillary tangles in amyotrophic lateral sclerosis/parkinsonism-dementia complex in the Kii peninsula of Japan. *J. Neuropathol. Exp. Neurol.* **62**, 791–798 (2003).
14. M. Hasegawa *et al.*, TDP-43 is deposited in the Guam parkinsonism-dementia complex brains. *Brain* **130**, 1386–1394 (2007).
15. J. Miklossy *et al.*, Enduring involvement of tau,  $\beta$ -amyloid,  $\alpha$ -synuclein, ubiquitin and TDP-43 pathology in the amyotrophic lateral sclerosis/parkinsonism-dementia complex of Guam (ALS/PDC). *Acta Neuropathol.* **116**, 625–637 (2008).
16. H. R. Morris *et al.*, Genome-wide analysis of the parkinsonism-dementia complex of Guam. *Arch. Neurol.* **61**, 1889–1897 (2004).
17. H. Tomiyama *et al.*, Mutation analyses in Amyotrophic Lateral Sclerosis/Parkinsonism-Dementia complex of the Kii peninsula, Japan. *Mov. Disord.* **23**, 2344–2348 (2008).
18. W. Sieh *et al.*, Identification of novel susceptibility loci for Guam neurodegenerative disease: Challenges of genome scans in genetic isolates. *Hum. Mol. Genet.* **18**, 3725–3738 (2009).
19. R. M. Garruto, D. C. Gajdusek, K. M. Chen, Amyotrophic Lateral Sclerosis and Parkinsonism-Dementia among Filipino migrants to Guam. *Ann. Neurol.* **10**, 341–350 (1981).
20. C. C. Plato *et al.*, Amyotrophic lateral sclerosis and Parkinsonism-Dementia complex of Guam: Changing incidence rates during the past 60 years. *Am. J. Epidemiol.* **157**, 149–157 (2003).
21. T. Cox, J. McDarby, L. Lavine, J. Steele, D. Calne, A Retinopathy on Guam with high prevalence in lytico-bodig. *Ophthalmology* **96**, 1731–1735 (1989).
22. Y. Kokubo, K. Ito, T. Fukunaga, H. Matsubara, S. Kuzuhara, Pigmentary retinopathy of ALS/PDC in Kii. *Ophthalmology* **113**, e1–e2 (2006).
23. M. Goedert, M. G. Spillantini, N. J. Cairns, R. A. Crowther, Tau proteins of Alzheimer paired helical filaments: Abnormal phosphorylation of all six brain isoforms. *Neuron* **8**, 159–168 (1992).
24. M. L. Schmidt, V. Zukareva, K. L. Newell, V. M.-Y. Lee, J. Q. Trojanowski, Tau isoform profile and phosphorylation state in dementia pugilistica. *Acta Neuropathol.* **101**, 518–524 (2001).
25. R. C. A. Pearson, M. M. Esiri, R. W. Hiorns, G. K. Wilcock, T. P. S. Powell, Anatomical correlates of the distribution of the pathological changes in the neocortex in Alzheimer disease. *Proc. Natl. Acad. Sci. U.S.A.* **82**, 4531–4534 (1985).
26. T. Tokuda, S. Ikeda, N. Yanagisawa, Y. Ihara, G. G. Glenner, Re-examination of ex-boxers' brains using immunohistochemistry with antibodies to amyloid- $\beta$  protein and tau protein. *Acta Neuropathol.* **82**, 280–285 (1991).
27. K. F. Bienek *et al.*, The second NINDS/NIBIB consensus meeting to define neuropathological criteria for the diagnosis of chronic traumatic encephalopathy. *J. Neuropathol. Exp. Neurol.* **80**, 210–219 (2021).
28. A. W. P. Fitzpatrick *et al.*, Cryo-EM structures of tau filaments from Alzheimer's disease. *Nature* **547**, 185–190 (2017).
29. B. Falcon *et al.*, Tau filaments from multiple cases of sporadic and inherited Alzheimer's disease adopt a common fold. *Acta Neuropathol.* **136**, 699–708 (2018).
30. B. Falcon *et al.*, Novel tau filament fold in chronic traumatic encephalopathy encloses hydrophobic molecules. *Nature* **568**, 420–423 (2019).
31. Y. Shi *et al.*, Structure-based classification of tauopathies. *Nature* **598**, 359–363 (2021).
32. G. I. Hallinan *et al.*, Structure of tau filaments in prion protein amyloidosis. *Acta Neuropathol.* **142**, 227–241 (2021).
33. C. Qi *et al.*, Identical Tau filaments in subacute sclerosing panencephalitis and chronic traumatic encephalopathy. *Acta Neuropathol. Commun.* **11**, 74 (2023).
34. J. Gutierrez, R. S. Issacson, B. S. Koppel, Subacute sclerosing panencephalitis: An update. *Dev. Med. Child Neurol.* **52**, 901–907 (2010).
35. H. Miyahara *et al.*, Independent distribution between tauopathy secondary to subacute sclerosing panencephalitis and measles virus. *Brain Pathol.* **32**, e13069 (2022).
36. Y. Yang *et al.*, Cryo-EM structures of amyloid- $\beta$  42 filaments from human brains. *Science* **375**, 167–172 (2022).
37. S. Taniguchi-Watanabe *et al.*, Biochemical classification of tauopathies by immunoblot, protein sequence and mass spectrometric analyses of sarkosyl-insoluble and trypsin-resistant tau. *Acta Neuropathol.* **131**, 267–280 (2016).
38. Y. Yang *et al.*, Structures of  $\alpha$ -synuclein filaments from human brains with Lewy pathology. *Nature* **610**, 791–795 (2022).
39. W. Zhang *et al.*, Novel tau filament fold in corticobasal degeneration. *Nature* **580**, 283–287 (2020).
40. T. Arakhamia *et al.*, Posttranslational modifications mediate the structural diversity of tauopathy strains. *Cell* **180**, 633–644 (2020).
41. S. H. W. Scheres, B. Ryskeldi-Falcon, M. Goedert, Molecular pathology of neurodegenerative diseases by cryo-EM of amyloids. *Nature* **621**, 701–710 (2023).
42. P. R. Hof *et al.*, Distribution of neurofibrillary tangles and senile plaques in the cerebral cortex in postencephalitic parkinsonism. *Neurosci. Lett.* **139**, 10–14 (1992).
43. M. S. Pollanen *et al.*, The spectrum of disease and tau pathology of nodding syndrome in Uganda. *Brain* **146**, 954–967 (2023).
44. S. Lövestam *et al.*, Assembly of recombinant tau into filaments identical to those of Alzheimer's disease and chronic traumatic encephalopathy. *eLife* **11**, e76494 (2022).
45. C. Condello *et al.*, Guam ALS-PDC is a distinct double-prion disorder featuring both tau and A $\beta$  prions. *Proc. Natl. Acad. Sci. U.S.A.* **120**, e2220984120 (2023).
46. M. Schweighauser *et al.*, Age-dependent formation of TMEM106B amyloid filaments in human brains. *Nature* **605**, 310–314 (2022).
47. J. Perneel *et al.*, Accumulation of TMEM106B C-terminal fragments in neurodegenerative disease and aging. *Acta Neuropathol.* **145**, 285–302 (2023).
48. M. L. Schmidt, R. Garruto, J. Chen, V. M.-Y. Lee, J. Q. Trojanowski, Tau epitopes in spinal cord neurofibrillary lesions in Chamorro of Guam. *Neuroreport* **11**, 3427–3430 (2000).
49. M. Goedert, R. Jakes, E. Vanmechelen, Monoclonal antibody A78 recognises tau protein phosphorylated at both serine 202 and threonine 205. *Neurosci. Lett.* **189**, 167–170 (1995).
50. H. Braak, E. Braak, T. Ohm, J. Bohl, Silver impregnation of Alzheimer's neurofibrillary changes counterstained for basophilic material and lipofuscin pigment. *Stain Technol.* **63**, 197–200 (2009).
51. D. Arseni *et al.*, Structure of pathological TDP-43 filaments from ALS with FTLD. *Nature* **601**, 139–143 (2022).
52. H. Guo *et al.*, Electron-event representation data enable efficient cryoEM file storage with full preservation of spatial and temporal resolution. *IUCr* **7**, 860–869 (2020).
53. S. He, S. H. W. Scheres, Helical reconstruction in RELION. *J. Struct. Biol.* **198**, 163–176 (2017).
54. J. Zivanov, T. Nakane, S. H. W. Scheres, A Bayesian approach to beam-induced motion correction in cryo-EM single particle analysis. *IUCr* **6**, 5–17 (2019).
55. A. Rohou, N. Grigorieff, CTFIND4: Fast and accurate defocus estimation from electron micrographs. *J. Struct. Biol.* **192**, 216–221 (2015).
56. S. H. W. Scheres, Amyloid structure determination in RELION-3.1. *Acta Crystallogr. D* **76**, 94–101 (2020).
57. J. Zivanov *et al.*, A Bayesian approach to single-particle electron cryo-tomography in RELION-4.0. *eLife* **11**, e83724 (2022).
58. S. H. W. Scheres, S. Chen, Prevention of overfitting in cryo-EM structure determination. *Nature Meth.* **9**, 853–864 (2012).
59. P. Emsley, B. V. Lohkamp, W. G. Scott, K. Cowtan, Features and development of Coot. *Acta Crystallogr. D* **66**, 486–501 (2010).
60. K. Yamashita, C. M. Palmer, T. Burnley, G. N. Murshudov, Cryo-EM single-particle structure refinement and map calculation using *Servalcat*. *Acta Crystallogr. D* **77**, 1282–1291 (2021).
61. G. N. Murshudov, A. Vagin, E. J. Dodson, Refinement of macromolecular structures by the maximum-likelihood method. *Acta Crystallogr. D* **53**, 240–255 (1997).
62. G. N. Murshudov *et al.*, REFMACS for the refinement of macromolecular crystal structures. *Acta Crystallogr. D* **67**, 355–367 (2011).
63. V. B. Chen *et al.*, MolProbity: All-atom structure validation for macromolecular crystallography. *Acta Crystallogr. D* **66**, 12–21 (2010).
64. E. F. Pettersen *et al.*, ChimeraX: Structure visualization for researchers, educators, and developers. *Protein Sci.* **30**, 70–82 (2021).
65. Qi *et al.*, EMD-17171, CTE Type I tau filament from Guam ALS/PDC. Electron Microscopy Data Bank. <https://www.ebi.ac.uk/emdb/EMD-17171>. Deposited 20 April 2023.
66. Qi *et al.*, EMD-17173, CTE Type III tau filament from Guam ALS/PDC. Electron Microscopy Data Bank. <https://www.ebi.ac.uk/emdb/EMD-17173>. Deposited 20 April 2023.
67. Qi *et al.*, EMD-17174, CTE Type II tau filament from Guam ALS/PDC. Electron Microscopy Data Bank. <https://www.ebi.ac.uk/emdb/EMD-17174>. Deposited 20 April 2023.
68. Qi *et al.*, EMD-17175, TMEM106B Fold I-s filament from Guam ALS/PDC. Electron Microscopy Data Bank. <https://www.ebi.ac.uk/emdb/EMD-17175>. Deposited 20 April 2023.
69. Qi *et al.*, EMD-17176, TMEM106B Fold I-d filament from Guam ALS/PDC. Electron Microscopy Data Bank. <https://www.ebi.ac.uk/emdb/EMD-17176>. Deposited 20 April 2023.
70. Qi *et al.*, EMD-17177, Ab42 TypeII filament from Guam ALS/PDC. Electron Microscopy Data Bank. <https://www.ebi.ac.uk/emdb/EMD-17177>. Deposited 20 April 2023.
71. Qi *et al.*, EMD-17178, CTE TypeI filament from Kii ALS/PDC. Electron Microscopy Data Bank. <https://www.ebi.ac.uk/emdb/EMD-17178>. Deposited 20 April 2023.
72. Qi *et al.*, EMD-17179, CTE TypeII filament from Kii ALS/PDC. Electron Microscopy Data Bank. <https://www.ebi.ac.uk/emdb/EMD-17179>. Deposited 20 April 2023.

73. Qi *et al.*, EMD-17180, CTE Type III filament from CTE case2. Electron Microscopy Data Bank. <https://www.ebi.ac.uk/emdb/EMD-17180>. Deposited 20 April 2023.
74. Qi *et al.*, EMD-17181, PHF filament from Kii ALS/PDC. Electron Microscopy Data Bank. <https://www.ebi.ac.uk/emdb/EMD-17181>. Deposited 20 April 2023.
75. Qi *et al.*, 8OT6, CTE Type I filament from Guam ALS/PDC. Protein Data Bank. <https://www.rcsb.org/structure/unreleased/8OT6>. Deposited 20 April 2023.
76. Qi *et al.*, 8OTC, CTE Type II filament from Guam ALS/PDC. Protein Data Bank. <https://www.rcsb.org/structure/unreleased/8OTC>. Deposited 20 April 2023.
77. Qi *et al.*, 8OT9, CTE Type III filament from Guam ALS/PDC. Protein Data Bank. <https://www.rcsb.org/structure/unreleased/8OT9>. Deposited 20 April 2023.
78. Qi *et al.*, 8OTD, TMEM106B Fold I-s filament from Guam ALS/PDC. Protein Data Bank. <https://www.rcsb.org/structure/unreleased/8OTD>. Deposited 20 April 2023.
79. Qi *et al.*, 8OTE, TMEM106B Fold I-d filament from Guam ALS/PDC. Protein Data Bank. <https://www.rcsb.org/structure/unreleased/8OTE>. Deposited 20 April 2023.
80. Qi *et al.*, 8OTF, Ab42 Type II filament from Guam ALS/PDC. Protein Data Bank. <https://www.rcsb.org/structure/unreleased/8OTF>. Deposited 20 April 2023.
81. Qi *et al.*, 8OTG, CTE Type I filament from Kii ALS/PDC. Protein Data Bank. <https://www.rcsb.org/structure/unreleased/8OTG>. Deposited 20 April 2023.
82. Qi *et al.*, 8OTH, CTE Type II filament from Kii ALS/PDC. Protein Data Bank. <https://www.rcsb.org/structure/unreleased/8OTH>. Deposited 20 April 2023.
83. Qi *et al.*, 8OTI, CTE Type III filament from CTE case2. Protein Data Bank. <https://www.rcsb.org/structure/unreleased/8OTI>. Deposited 20 April 2023.
84. Qi *et al.*, 8OTJ, PHF filament from Kii ALS/PDC. Protein Data Bank. <https://www.rcsb.org/structure/unreleased/8OTJ>. Deposited 20 April 2023.